Journal of Power Sources 185 (2008) 1398–1407

Contents lists available at ScienceDirect

Journal of Power Sources

journal homepage: www.elsevier.com/locate/jpowsour

Thermodynamic model development for lithium intercalation electrodes

Deepak K. Karthikeyan, Godfrey Sikha, Ralph E. White*

Center for Electrochemical Engineering, Department of Chemical Engineering, University of South Carolina, Columbia, SC 29208, USA

ARTICLE INFO

Article history:
Received 5 June 2008
Received in revised form 18 July 2008
Accepted 21 July 2008
Available online 5 August 2008

Keywords:
Intercalation electrodes
Equilibrium potential
Nernst equation
Activity correction factor
Single particle model

ABSTRACT

Staging is a characteristic phenomena observed in intercalation electrodes. During staging process the equilibrium potential of the electrode exhibits weak dependence on the solid phase Li concentration and does not follow the classical Nernst behavior. The coexistence of structurally different solid phases results in multiple plateaus in the equilibrium potential curve. Such complexities make the thermodynamic description of equilibrium potential as a function of concentration difficult, and so it is usually represented through an empirical expression. The objective of this work is to develop a frame work based on thermodynamic principles to describe the equilibrium potential of intercalation electrodes. Redlich-Kister thermodynamic equation was used to describe the excess Gibbs free energy, which in turn was used to evaluate the equilibrium potential as a function of concentration. The equilibrium potential expression for different lithium intercalation electrodes such as $LiCoO_2$, $LiNi_{0.8}Co_{0.15}Al_{0.05}O_2$, graphite and hard carbon were developed based on Redlich-Kister equation. The thermodynamic model was also used to estimate the activity of species directly from excess Gibbs free energy. The developed thermodynamic expressions along with the activity correction are incorporated into a single particle diffusion model for a Li-ion cell consisting of a graphite and $LiCoO_2$ electrode. The interactions between the Li-ions during intercalation/deintercalation process were incorporated into the present model by considering the chemical potential gradient corrected for activity as the driving force. The effect of inclusion of activity correction in the single particle model was studied for different discharge rates. It was observed that the activity correction term yielded increased capacity especially at higher rates. The effect of activity correction term was also found to be more significant in the $LiCoO_2$ electrode compared to the carbon electrode.

1. Introduction

The equilibrium potential of the Li-ion intercalation electrodes does not follow Nernst equation, due to the solid state redox reaction. This characteristic anomalous voltage behavior had been studied and discussed extensively in literatures [1–8]. Due to the lack of understanding of the solid state redox reactions, the experimental equilibrium potential profile is usually fitted to a empirical expression which was then used for model predictions [9–11]. Some of the earlier models used modified Nernst equation to predict equilibrium potential as in the case of Li/TiS_2 system developed by West et al. [1]. Verburgge and Koch [2] derived a thermodynamic correlation to describe the equilibrium potential associated with a single fiber of a partially graphitic carbon electrode. This equation is based on the excess Gibbs free energy given by Wohl's function to represent the deviation from ideal solution behavior. Later, Zhang et al. [12] extended Verburgge and Koch [3] approach to model the lithiated carbon anode and metal oxide cathode. In this model, Nernst equation was raised to a suitable power to represent individual voltage plateaus. The shape of the equilibrium potential curve depends on the value chosen for the exponential factor. For a smaller value, it reduces the exponential dependence of concentration in the Nernst equation so as to give a flat equilibrium potential profile. However the Li-ion interactions, which cause the flat plateau in the equilibrium potential profile [4], were not considered in their model.

Previous studies on Nickel electrode have shown that the equilibrium potential can be modeled based on the thermodynamics of the non-ideal solutions [13–15]. Ali, used a simple one parameter Margules equation for the excess free energy to predict the equilibrium potential along with the temperature effects for $LiMn_2O_4$ electrode [8]. In this work, the equilibrium potential of insertion electrodes was modeled using excess functions by applying the principles of thermodynamics of non-ideal solutions. Thermodynamic equations such as one parameter Margules, two parameter Margules, van Laar and Redlich-Kister equations were used to describe the non-ideal behavior and were compared with the experimental equilibrium potential data for various intercalation

* Corresponding author. Tel.: +1 803 777 3270; fax: +1 803 777 6769.
E-mail address: white@engr.sc.edu (R.E. White).

0378-7753/$ – see front matter © 2008 Elsevier B.V. All rights reserved.
doi:10.1016/j.jpowsour.2008.07.077

Nomenclature

a	activity of species
A	parameter of 1 parameter Margules equation ($J\,mol^{-1}$)
A_0, B_0	parameter of 2 parameter Margules equation ($J\,mol^{-1}$)
A'_0, B'_0	parameter of van Laar equation ($J\,mol^{-1}$)
A_0, A_1, A_2	interaction parameter in Redlich-Kister equation ($J\,mol^{-1}$)
c_e	concentration of the electrolyte ($mol\,cm^{-3}$)
$C_{s,i,max}$	maximum concentration ($mol\,cm^{-3}$)
$D_{\alpha,i}$	diffusion coefficient ($cm^2\,s^{-1}$)
D_{eff}	effective diffusivity ($cm^2\,s^{-1}$)
F	Faradays constant ($96485\,C\,mol^{-1}$)
$\overline{g}^E$	partial molar excess free energy
G_E	excess Gibbs free energy ($J\,mol^{-1}$)
I	identity matrix
I_{app}	applied current (A)
J	Jacobian matrix
J^T	Jacobian transpose
k_i	rate constant of the electrochemical reaction ($cm^{2.5}\,mol^{-0.5}\,s^{-1}$)
N	denotes number of parameter in the Redlich-Kister equation
$N_{\alpha,i}$	flux of lithium ions ($mol\,cm^{-3}$)
R	ideal gas constant ($8.314\,J\,mol^{-1}\,K^{-1}$)
R_i	radius of the electrode particle (cm)
$\tilde{R}$	dimensionless radius
s_i	active electrode area (cm^2)
t	time (s)
T	temperature (K)
U	equilibrium potential (V)
U_0	standard equilibrium potential (V)
V_{INT}	non-ideal Nernst correction term (V)
w_i	electrode loading ($g\,cell^{-1}$)
x	mole fraction
Y_i	experimental data vector
Y^*	predicted data vector

Greek letters

β	transfer coefficient
γ	activity coefficient
η_s	surface over potential (V)
θs	vacant site in the host material
λ	step size correction factor
μ	chemical potential ($J\,mol^{-1}$)
ρ_i	density of the active material ($g\,cm^{-3}$)
ϕ_i	solid phase potential (V)
ϕ_e	solution phase potential (V)

Superscript

0	standard state

Subscript

i	denoted p or n
n	negative electrode
p	positive electrode
s	host material
α	intercalating species (lithium ion)
β	vacant site in the host material

electrodes like $LiCoO_2$, $LiNi_{0.8}Co_{0.15}Al_{0.05}O_2$, graphite and hard carbon. The Redlich-Kister equation was identified to be a consistent methodology to fit the equilibrium potentials of all electrodes that were studied. The activity correction term introduced by the non-ideality was evaluated from the excess free energy developed through Redlich-Kister equation. The activity correction term which takes into account for the non-ideal interactions, varies with respect to the concentration of Li-ion in the intercalation electrode [2,16]. The activity corrected thermodynamic expression was used to describe the open-circuit potential for graphite and $LiCoO_2$, in a lithium-ion single particle battery model.

2. Experiment

The equilibrium potential curves for different electrodes studies were measured using a coin cell setup. The equilibrium potential measurements were made at room temperature for $LiCoO_2$, meso-carbon micro-beads (MCMB), $LiNi_{0.8}Co_{0.15}Al_{0.05}O_2$, hard carbon electrodes. The lithium cobalt oxide and MCMB electrodes were provided by Mine Safety Appliances Company (Sparks, MD), $LiNi_{0.8}Co_{0.15}Al_{0.05}O_2$ and hard carbon electrodes were provided by Quallion LLC (Sylmar, CA) and MeadWestvaco Corporation (Charleston, SC), respectively. A Celgard 2400 polypropylene membrane (Charlotte, NC) was used as the separator, Lithium metal foil from FMC Corporation (Bessemer city, NC) was used as a reference electrode. The electrolyte used was 1 M $LiPF_6$ in a 1:1 v/v solution of ethylene carbonate-dimethyl carbonate provided by Ferro (Independence, OH). The cells were assembled in an argon filled glove box. Both the working and the counter electrode were made by punching out circular disc of 5/8th″ diameter. While a circular separator sheet of 3/4th″ was used to separate both the electrodes. The electrolyte was added sufficiently so as to wet separator and the electrodes; finally the cell was sealed firmly.

Following an initial rest of 24 h, the cells were cycled in a 16 channel Arbin test station (Arbin Instruments, College Station, TX) for at least five cycles before equilibrium potential measurements were made. After the initial cycles, the cells were allowed to discharge, from completely charged state at a very slow rate of C/30. The equilibrium potential was recorded with respect to the capacity, from which the stoichiometric coefficient of lithium was calculated as the ratio of the difference between the total discharge capacity and discharge capacity at a particular time to that of the theoretical capacity of the intercalation electrode.

3. Thermodynamic Model Development

Derivation of the equilibrium potential for insertion electrodes:

The reaction at the interface of the electrolyte and the solid phase [2,17] is given by:

$$Li^+ + e^- + \theta_s \rightleftharpoons [Li^{\delta} - \theta_s^{-\delta}] \quad (1)$$

where θ_s is a vacant site available for Li-ions to intercalate into the host material, denoted by subscript β throughout this article. The host material may be the carbon or the metal oxide electrode. Similarly $[Li^{\delta} - \theta_s^{-\delta}]$ represents the intercalated species, denoted by α. Even after insertion the Li-ion retains the significant positive charge (δ) and the host site retains a negative charge ($-\delta$), evidenced by X-ray photoelectron spectroscopy analysis (XPS) [18].

In general, from a thermodynamic perspective, the equilibrium potential of the intercalation electrode relative to a reference Li electrode is given by [17]:

$$FU = \mu^0_{Li} + \mu_\beta - \mu_\alpha \quad (2)$$

where μ_i is the chemical potential of the species i corresponding to an infinitely dilute solution. μ^0_{Li} is the chemical potential of pure lithium metal, which is independent of the composition of the host material. Subscript α represents the lithium intercalated host material, β denoted unoccupied host material. The chemical potential is expressed in terms of the activity coefficient (γ_i), mole fraction (x_i) and secondary reference chemical potential (μ^0_i) as [17,19]

$$\mu_i = \mu_i^0 + RT\ln(\gamma_i x_i) \tag{3}$$

R and T are the ideal gas constant and the temperature, respectively. Substituting Eq. (3) in (2), we obtain:

$$\begin{aligned} FU &= \mu^0_{Li} + \mu^0_\beta - \mu^0_\alpha + RT\ln\left(\frac{x_\beta}{x_\alpha}\right) + RT\ln\left(\frac{\gamma_\beta}{\gamma_\alpha}\right) \\ &= FU^0 + RT\ln\left(\frac{x_\beta}{x_\alpha}\right) + RT\ln\left(\frac{\gamma_\beta}{\gamma_\alpha}\right) \end{aligned} \tag{4}$$

The deviation from the ideal behavior represented by the last term on the right hand side of the Eq. (4) is due to the pseudo binary interactions between the Li-ion and the host matrix the during intercalation/deintercalation process. In case of unit activity (ideal condition) Eq. (4) takes the form of classical Nernst equation [20] given by:

$$FU = FU^0 + RT\ln\left(\frac{x_\beta}{x_\alpha}\right) \tag{5}$$

where U^0 is the standard equilibrium potential, s_i is the stoichiometric coefficient and c_i is related to the concentration of the species i. The activity coefficient by definition in Eq. (4) is related to Gibbs partial molar excess free energy [19]:

$$RT\ln\gamma_\alpha = \bar{g}^E_\alpha = \frac{\partial}{\partial n_\alpha}(n_t G_E)_{T,P,j\neq\alpha} \tag{6}$$

$$RT\ln\gamma_\beta = \bar{g}^E_\beta = \frac{\partial}{\partial n_\beta}(n_t G_E)_{T,P,j\neq\beta} \tag{7}$$

where n_t is the total number of moles of α and β species ($n_t = n_\alpha + n_\beta$). G_E is the excess Gibbs free energy. At a fixed temperature and pressure the excess free energy of a mixture with respect to the composition can be calculated from thermodynamic equations such as one parameter Margules, two parameter Margules, van Laar or Redlich-Kister equations [19,21]. In this paper, these models are compared with the experimental equilibrium potential data.

In a binary mixture when the excess properties are taken with reference to an ideal solution, the molar excess Gibbs free energy must obey the two boundary conditions:

$$\begin{aligned} &G_E \to 0 \quad \text{when } x_\alpha \to 0 \\ &G_E \to 0 \quad \text{when } x_\beta \to 0 \end{aligned} \tag{8}$$

A simple expression that obeys this boundary condition is the one parameter Margules equation, given by [21]:

$$\begin{aligned} G_E &= RT A x_\alpha x_\beta \\ &= RT A x_\alpha(1-x_\alpha) \end{aligned} \tag{9}$$

The mole fraction of the intercalating species x_α is the ratio of the moles of α species (n_α) to that of the total number of moles (n_t), $x_\alpha = n_\alpha/(n_\alpha + n_\beta)$. Similarly the mole fraction of the host matrix x_β is given as $x_\beta = n_\beta/(n_\alpha + n_\beta)$.

Substituting Eq. (9), x_α, x_β in Eqs. (6) and (7), differentiating with respect to n_α and n_β, the following expressions for the activity coefficients are obtained as

$$\begin{aligned} &\ln(\gamma_\alpha) = A(1-x_\alpha)^2 \\ &\ln(\gamma_\beta) = Ax_\alpha^2 \end{aligned} \tag{10}$$

where A is the interaction parameter with the units of energy, which is characteristic of components and depends upon the temperature and independent of concentration.

The equilibrium potential is derived from Eqs. (4) and (10):

$$FU = FU^0 + RT\ln\left(\frac{1-x_\alpha}{x_\alpha}\right) + RT[\ln(\gamma_\beta) - \ln(\gamma_\alpha)] \tag{11}$$

$$FU = FU^0 + RT\ln\left(\frac{1-x_\alpha}{x_\alpha}\right) + RT[A(2x_\alpha - 1)] \tag{12}$$

The activity coefficients for the other models are calculated using a similar procedure, and using these values the equilibrium potential is obtained.

The excess Gibbs free energy for two parameter Margules equation is given by [19]:

$$\begin{aligned} G_E &= RTx_\alpha x_\beta[A_0 x_\alpha + B_0 x_\beta] \\ &= RTx_\alpha(1-x_\alpha)[A_0 x_\alpha + B_0(1-x_\alpha)] \end{aligned} \tag{13}$$

The activity coefficients for two parameter Margules equation is derived as

$$\begin{aligned} \ln(\gamma_\alpha) &= \left(A_0 - \frac{3}{2}B_0\right)x_\alpha^2 + B_0 x_\alpha^3 \\ \ln(\gamma_\beta) &= A_0(1-x_\alpha)^2 + B_0(1-x_\alpha)^3 \end{aligned} \tag{14}$$

A_0 and B_0 are the interaction parameters for the two parameter Margules equation. Equilibrium potential from Eqs. (4) and (14) is given as

$$\begin{aligned} FU = FU^0 &+ RT\ln\left(\frac{1-x_\alpha}{x_\alpha}\right) \\ &+ RT\left[-A_0 + 2A_0x_\alpha - B_0 + 3B_0x_\alpha - \frac{3}{2}B_0x_\alpha^2\right] \end{aligned} \tag{15}$$

The expression for excess Gibbs free energy proposed by van Laar is given by [21]:

$$\begin{aligned} G_E &= \frac{RT}{[1/A'_0x_\alpha + 1/B'_0x_\beta]} \\ &= \frac{RT}{[1/A'_0x_\alpha + 1/B'_0(1-x_\alpha)]} \end{aligned} \tag{16}$$

where A'_0, B'_0 are the interaction parameters of the van Laar equation. The activity coefficients of the intercalating species (γ_α) and the host material (γ_β) are derived from Eqs. (6) and (7) by substituting them in the expression for the excess Gibbs free energy.

$$\begin{aligned} \ln(\gamma_\alpha) &= \frac{A'_0(1-x_\alpha)^2}{[(1-x_\alpha) + B'_0x_\alpha]^2} \\ \ln(\gamma_\beta) &= \frac{A'_0B'_0x_\alpha^2}{[(1-x_\alpha) + B'_0x_\alpha]^2} \end{aligned} \tag{17}$$

From the activity coefficients, the equilibrium potential is derived as

$$FU = FU^0 + RT\ln\left(\frac{1-x_\alpha}{x_\alpha}\right) + RT\left[\frac{A'_0(B'_0x_\alpha^2 - 1 + 2x_\alpha - x_\alpha^2)}{(1-x_\alpha + B'_0x_\alpha)^2}\right] \tag{18}$$

The excess Gibbs free energy according to Redlich-Kister expansion is given by [19]:

$$G_E = x_{\alpha,i}x_{\beta,i}\sum_{k=0}^{N}A_k(x_{\alpha,i} - x_{\beta,i})^k \tag{19}$$

$$G_E = x_{\alpha,i}(1-x_{\alpha,i})\sum_{k=0}^{N}A_k(2x_{\alpha,i} - 1)^k \tag{20}$$

Substituting Eqs. (20) in (6) and (7), and using the expression for x_α and x_β, the activity coefficients are derived as

$$RT \ln \gamma_{\alpha,i} = \sum_{k=0}^{N} A_k (1 - x_{\alpha,i})^2 (2x_{\alpha,i} - 1)^k \left[\frac{2x_{\alpha,i} k}{(2x_{\alpha,i} - 1)} + 1 \right] \quad (21)$$

$$RT \ln \gamma_{\beta,i} = \sum_{k=0}^{N} A_k x_{\alpha,i}^2 (2x_{\alpha,i} - 1)^k \left[1 - \frac{2k(1 - x_{\alpha,i})}{(2x_{\alpha,i} - 1)} \right] \quad (22)$$

Substituting the above Eqs. (21) and (22) in the equilibrium potential (4) gives:

$$FU = FU^0 + RT \ln \left(\frac{x_{\beta,i}}{x_{\alpha,i}} \right) + \left\{ \sum_{k=0}^{N} A_k \cdot \left[(2x_{\alpha,i} - 1)^{k+1} - \frac{2x_{\alpha,i} k(1 - x_{\alpha,i})}{(2x_{\alpha,i} - 1)^{1-k}} \right] \right\} \quad (23)$$

$$FU = FU^0 + RT \ln \left(\frac{1 - x_{\alpha,i}}{x_{\alpha,i}} \right) + V_{\text{INT}} \quad (24)$$

V_{INT} is the non-ideal interaction term,

$$V_{\text{INT}} = \left\{ \sum_{k=0}^{N} A_k \left[(2x_{\alpha,i} - 1)^{k+1} - \frac{2x_{\alpha,i} k(1 - x_{\alpha,i})}{(2x_{\alpha,i} - 1)^{1-k}} \right] \right\} \quad (25)$$

The expressions in Table 1 give the equations for the equilibrium potential of the Li-ion intercalation electrodes. By knowing the interaction parameters, the activity coefficient of the two species involved in the binary interactions [19] can be calculated.

4. Parameter Estimation

The parameters in the expression for the equilibrium potential are determined using Levenberg Marquardt method. It is an interpolation technique between the Gauss–Newton and the steepest descent method [22]. The correction vector $\Delta\theta$ is defined as follows:

$$\Delta\theta = (J^{\mathrm{T}} J + \lambda I)^{-1} J^{\mathrm{T}} (Y^* - Y_i) \quad (26)$$

where J is the Jacobian matrix of partial derivative of dependent variable in the model (i.e.) equilibrium potential with respect to the estimated parameter values evaluated at the experimental data points. $(Y^* - Y_i)$ represents the difference between the model prediction and the observed data vector. The value of convergence factor λ is chosen for each iteration, according to that the corrected parameter vector will result in a lower sum of squares error in the following iteration. This technique is explained in detail in Ref. [22].

5. Results and Discussion

The measured equilibrium potentials of MCMB and Hard carbon are shown in Fig. 1. In the case of the MCMB anode, the equilibrium potential has flat plateau regions due to characteristic staging phenomena [5,23,24], and in case of hard carbon the equilibrium potential profile was a smooth function [2,16], with respect to the stoichiometric coefficient. Fig. 2 shows the equilibrium potential for $LiCoO_2$ and $LiNi_{0.8}Co_{0.15}Al_{0.05}O_2$, the stoichiometric coefficient for $LiCoO_2$ starts approximately from 0.4 below which Li cannot be reversibly removed. The experimental data were fitted to the model Eqs. (12), (15), (18) and (23) shown in Table 1. Using the parameter estimation technique described

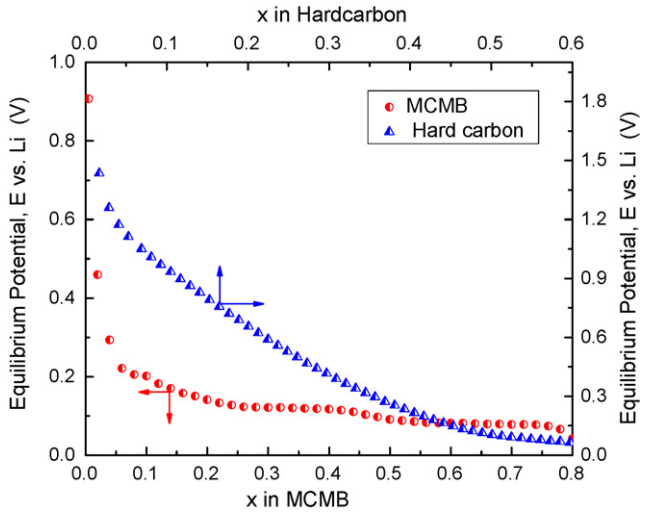

Fig. 1. Equilibrium potential vs. Li (V) as a function of stoichiometric coefficient for MCMB and hard carbon.

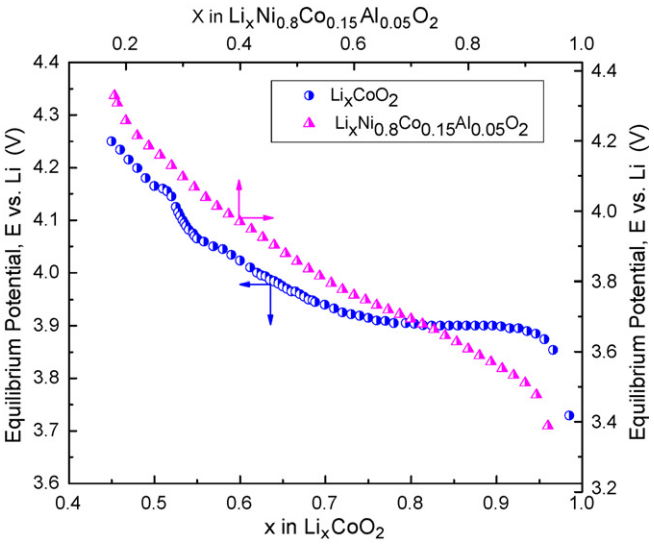

Fig. 2. Equilibrium potential vs. Li (V) as a function of stoichiometric coefficient for $LiCoO_2$, and $LiNi_{0.8}Co_{0.15}Al_{0.05}O_2$.

Table 1
Model equations for equilibrium potential using various equations of state

One parameter Margules	$FU = FU^0 + RT \ln \left(\frac{1-x_\alpha}{x_\alpha} \right) + RT[A(2x_\alpha - 1)]$
Two parameter Margules	$FU = FU^0 + RT \ln \left(\frac{1-x_\alpha}{x_\alpha} \right) + RT \left[-A_0 + 2A_0 x_\alpha - B_0 + 3B_0 x_\alpha - \frac{3}{2} B_0 x_\alpha^2 \right]$
van Laar equation	$FU = FU^0 + RT \ln \left(\frac{1-x_\alpha}{x_\alpha} \right) + RT \left[\frac{A'_0 (B'_0 x_\alpha^2 - 1 + 2x_\alpha - x_\alpha^2)}{(1 - x_\alpha + B'_0 x_\alpha)^2} \right]$
Redlich-Kister expansion	$FU = FU^0 + RT \ln \left(\frac{1-x_{\alpha,i}}{x_{\alpha,i}} \right) + \left\{ \sum_{k=0}^{N} A_k \cdot \left[(2x_{\alpha,i} - 1)^{k+1} - \frac{2x_{\alpha,i} k(1-x_{\alpha,i})}{(2x_{\alpha,i} - 1)^{1-k}} \right] \right\}$

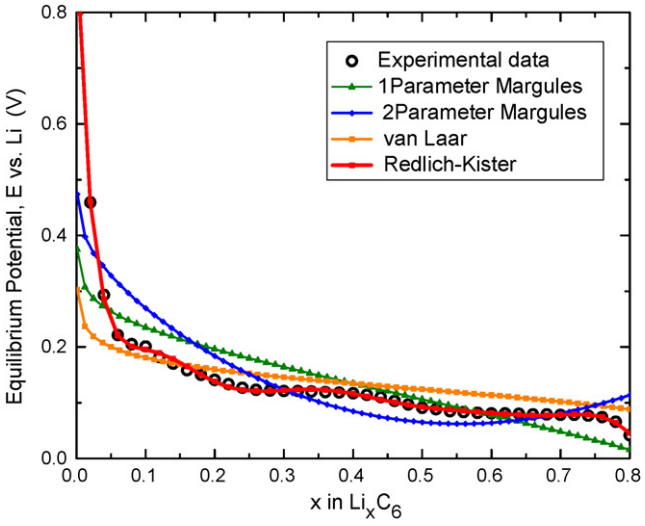

Fig. 3. Comparison of the experimental data with the model predictions for the equilibrium potential of MCMB using the equations in Table 1.

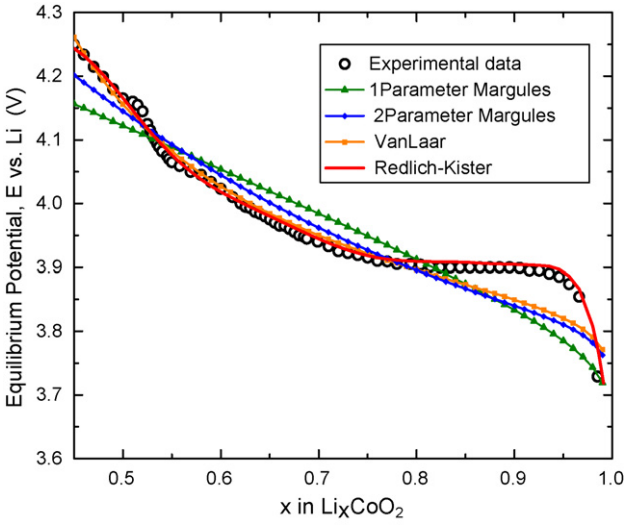

Fig. 5. Comparison of the experimental data with the model predictions for the equilibrium potential of $LiCoO_2$ using the equations in Table 1.

before, the interaction parameters in the model equations were determined. Fig. 3 compares the experimental potential profile of MCMB with that of the model predictions from all three expressions (Margules, van Laar, Redlich-Kister equation). The Margules expressions and the van Laar equation displayed a poor fit to the experimental data, which indicates that one or two interaction parameters to predict the non-ideal nature of the equilibrium potential of the MCMB electrode is not possible. The plot also shows the Redlich-Kister Eq. (23) fit to the experimental data, for $N = 11$ gave a good fit to the data throughout the entire stoichiometric region. In case of hard carbon (Fig. 4) the predictions from the two parameter Margules and the van Laar equations shows reasonable agreement with the experimental data. The fits become poor when the stoichiometric coefficient is less than 0.1. However the use of Redlich-Kister equation (with $N = 5$) gives an accurate fit over the entire stoichiometric region. It was also clear that a higher value for N is required in the case of MCMB which exhibits several voltage plateaus than when compared to hard carbon.

A similar trend was observed in fitting the equilibrium potential of the positive electrodes. $LiCoO_2$ gives a voltage plateau [25–27] after $x = 0.75$. Neither the Margules nor the van Laar equation was able to fit accurately in the plateau regions, while Redlich-Kister equation with $N = 7$ predict the plateau region accurately as shown in Fig. 5. Similar comparison was made for the experimental equilibrium profile for $LiNi_{0.8}Co_{0.15}Al_{0.05}O_2$ cathode as shown in Fig. 6, using $N = 5$ in the Redlich-Kister equation gave the best fit. The estimated parameter values are reported in Tables 2–7 the along with the 95% confidence intervals. The confidence intervals of all the parameters are well with in the limits of the actual parameters.

The parameters A, B, A^0, B^0, A_k, are the binary interaction parameters which represent the interactions between Li-ion during intercalation (or deintercalation). They have the unit of energy and a linear dependence on temperature, but were independent of composition [19]. The number of parameters required to represent the excess free energy of a binary mixture gives an indication of the complexity of the mixture, which provides a methodology for their

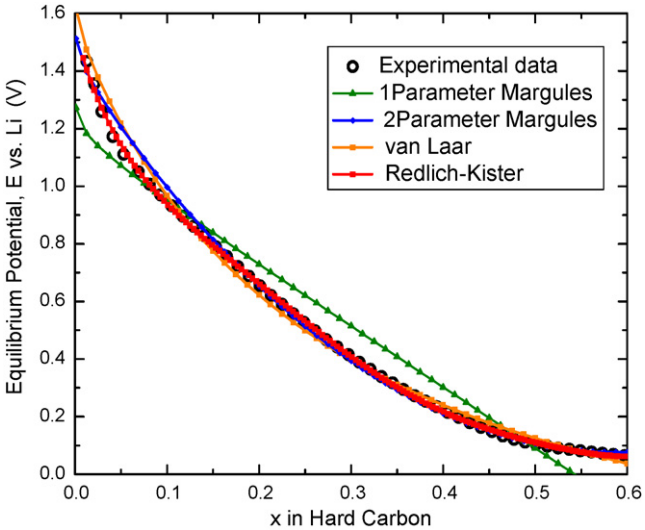

Fig. 4. Comparison of the experimental data with the model predictions for the equilibrium potential of MCMB using the equations in Table 1.

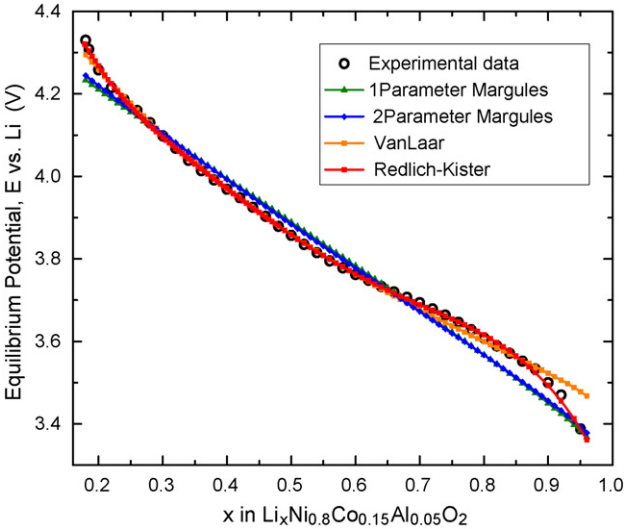

Fig. 6. Comparison of the experimental data with the model predictions for the equilibrium potential of hard carbon using the equations in Table 1.

Table 2
Parameter values obtained along with 95% confidence intervals for MCMB

Parameters	1P Margules	2P Margules	van Laar
U_0	0.10606 ± 0.00318	0.14262 ± 0.003612	0.12391 ± 0.0031484
A	−3.4990 ± 0.24424	18.009 ± 1.2985	$0.22646 \times 10^{-6} \pm 0.14947 \times 10^{-5}$
B	–	−23.954 ± 1.425	−4.0182 ± 0.0074410

Table 3
Parameter values obtained along with 95% confidence intervals for hard carbon

Parameters	1P Margules	2P Margules	van Laar
U_0	0.08996 ± 0.01019	0.4220 ± 0.01061	0.27205 ± 0.00404
A	−38.911 ± 0.75552	62.236 ± 2.9399	−45.400 ± 0.40939
B	–	−97.675 ± 2.8202	2.9729 ± 0.066553

Table 4
Parameter values obtained along with 95% confidence intervals for $LiCoO_2$

Parameters	1P Margules	2P Margules	van Laar
U^0	4.1222 ± 0.001933	4.2217 ± 0.0056795	3.1238 ± 0.19788
A	−11.222 ± 0.13779	−1.3060 ± 0.55032	−301.38 ± 141.51
B	–	−23.761 ± 1.2789	−10.190 ± 2.1697

Table 5
Parameter values obtained along with 95% confidence intervals for $LiNi_{0.8}Co_{0.15}Al_{0.05}O_2$

Parameters	1P Margules	2P Margules	van Laar
U^0	3.8887 ± 0.0031031	3.8927 ± 0.0038887	3.9261 ± 0.00445
A	−18.457 ± 0.25185	−16.676 ± 1.0875	−26.456 ± 1.0995
B	–	−2.7731 ± 1.6476	−1.7298 ± 0.8707

Table 6
Parameter values using Redlich-Kister equation for Hard carbon and $LiNi_{0.8}Co_{0.15}Al_{0.05}O_2$

Parameters	Hard carbon	$LiNi_{0.8}Co_{0.15}Al_{0.05}O_2$
N	5	5
U_0	2.0399 ± 0.7093	3.9662 ± 0.0240
A_0	$2.8601 \times 10^5 \pm 1.368 \times 10^5$	$-5.8992 \times 104 \pm 4.3067 \times 10^3$
A_1	$3.7239 \times 10^5 \pm 1.3679 \times 10^5$	$-2.0881 \times 104 \pm 4.8703 \times 10^3$
A_2	$3.1869 \times 10^5 \pm 1.3942 \times 10^5$	$-1.3273 \times 104 \pm 3.2012 \times 10^3$
A_3	$3.3667 \times 10^5 \pm 1.4315 \times 10^5$	$-6.9538 \times 103 \pm 4.3707 \times 10^3$
A_4	$3.3619 \times 10^5 \pm 1.1517 \times 10^5$	$-2.6023 \times 104 \pm 1.0753 \times 10^4$
A_5	$1.7017 \times 10^5 \pm 4.4532 \times 10^4$	$1.0715 \times 104 \pm 1.2839 \times 10^4$

classification. If for example only one parameter was required to describe the system, then the solution could be classified as simple, whereas if four or more parameter was required to describe a system, the mixture was denoted as a complex system. In case of insertion electrodes of all types it requires at least five parameters and therefore considered to be complex mixtures.

Table 7
Parameter values using Redlich-Kister equation for LiC_6 and $LiCoO_2$

Parameters	MCMB	$LiCoO_2$
N	10	7
U_0	−1.7203 ± 0.51308	−29.614 ± 2.3806
A_0	$-0.35799 \times 10^6 \pm 0.99032 \times 10^5$	$0.64832 \times 10^7 \pm 0.45934 \times 10^6$
A_1	$-0.35008 \times 10^6 \pm 0.99055 \times 10^5$	$-0.65173 \times 10^7 \pm 0.45933 \times 10^6$
A_2	$-0.35247 \times 10^6 \pm 0.98397 \times 10^5$	$0.65664 \times 10^7 \pm 0.45969 \times 10^6$
A_3	$-0.35692 \times 10^6 \pm 0.97652 \times 10^5$	$-0.65787 \times 10^7 \pm 0.46137 \times 10^6$
A_4	$-0.38633 \times 10^6 \pm 0.10929 \times 10^6$	$0.63021 \times 10^7 \pm 0.44922 \times 10^6$
A_5	$-0.35908 \times 10^6 \pm 0.11797 \times 10^6$	$-0.50465 \times 10^7 \pm 0.37283 \times 10^6$
A_6	$-0.28794 \times 10^6 \pm 0.52429 \times 10^5$	$0.27113 \times 10^7 \pm 0.21054 \times 10^6$
A_7	$-0.14979 \times 10^6 \pm 0.80161 \times 10^5$	$-0.69045 \times 10^6 \pm 0.56136 \times 10^5$
A_8	$-0.39912 \times 10^6 \pm 0.20291 \times 10^6$	
A_9	$-0.96172 \times 10^6 \pm 0.31894 \times 10^6$	
A_{10}	$-0.63262 \times 10^6 \pm 0.14748 \times 10^6$	

According to Shain's calculations [19] the interaction parameters in the Redlich-Kister equation (A_k) affects the miscibility and the phase separation of the binary mixture. A large positive value of A_0 favors limited miscibility. A small positive value of the parameter A_2 tends to decrease the phase separation. Another advantage of this procedure is that the activity correction term $[1 + (\mathrm{d} \ln \gamma_{\alpha,i} / \mathrm{d} \ln x_{\alpha,i})]$ is determined by using the non-ideal thermodynamic expression and partial Gibbs free energy to fit the equilibrium potential data. The activity correction term is used to correct the solid phase diffusion coefficient, which changes during intercalation as the function of the concentration of Li-ions.

In the next section single particle model was developed using MCMB and $LiCoO_2$ electrodes. In order to check the goodness of the fit, error estimation analysis was carried out for the two electrodes. Fig. 7 shows that the predicted value for the equilibrium potential agrees well with in the limits of the experimental data. Increasing the number of parameters can further minimize the errors but the confidence intervals for the parameters will be higher. Hence the number of parameters was selected in such a way that it minimized the error without increasing the confidence intervals. The system was tested by applying Gibbs-Duhem equation, which relates the activity coefficients of all components in a mixture. It must be valid for the estimated parameters [19], given by

$$\sum_i x_i \, \mathrm{d}\, \mu_i = 0 \tag{27}$$

In case of a binary mixture at constant temperature and pressure, the Gibbs-Duhem equation can be written as follows:

$$x_\alpha \frac{\mathrm{d} \ln \gamma_\alpha}{\mathrm{d}x_\alpha} = x_\beta \frac{\mathrm{d} \ln \gamma_\beta}{\mathrm{d}x_\beta} \tag{28}$$

Eq. (28) is used to determine the consistency of the parameters obtained for LiC_6 and $LiCoO_2$. The parameters from Table 8 are

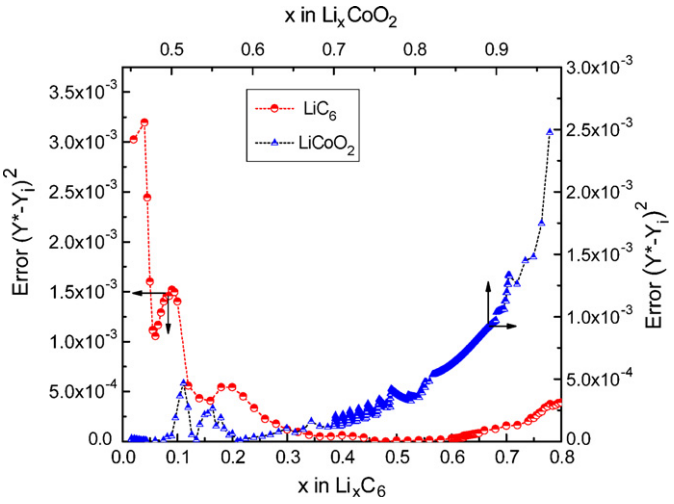

Fig. 7. Error estimates between the experimental and the predicted value for LiC_6 and $LiCoO_2$ electrodes.

Table 8
Cell parameters used in single particle model

Parameters	Cathode (i = p)	Anode (i = n)
$C_{s,i,max}$ (mol cm^{-3})	5.1555×10^{-2}	3.055×10^{-2}
R_i (cm)[a]	11.0×10^{-4}	12.5×10^{-4}
w_i (g cell^{-1})[a]	15.92	7.472
ρ_i (g cm^{-3})[a]	5.01	2.26
D_i (cm^2 s^{-1})[b]	1×10^{-10}	3.9×10^{-14}
$s_i(3w_i/R_i\rho_i)$(cm^2)	8666.3	7934.9
k_i (mol/cm^2 s/(mol/cm^3)$^{1.5}$)[b] $\equiv$ (cm$^{2.5}$ mol$^{-0.5}$ s^{-1})	5.03×10^{-6}	2.33×10^{-6}
c_e (mol cm^{-3})[a]	1×10^{-3}	
R (J mol^{-1} K^{-1})	8.314	
F (C mol^{-1})	96487	

[a] Ref. [31].
[b] Ref. [30].

substituted in Eqs. (21) and (22). On differentiating those equations with respect to their corresponding compositions both sides of Eq. (28) can be determined, the result for MCMB electrode was shown in Fig. 8. The two curves are the mirror image of each

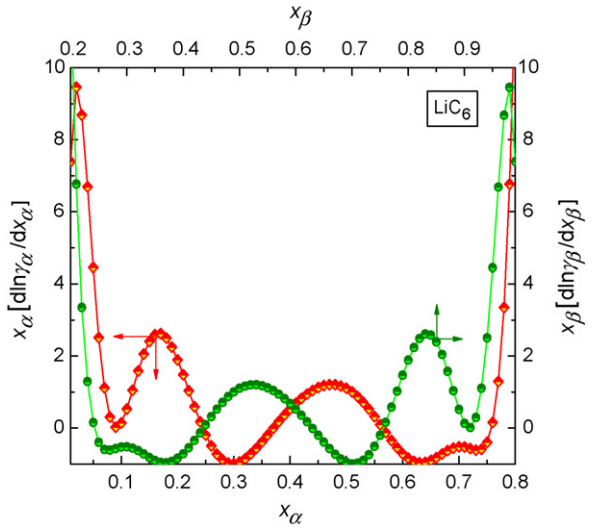

Fig. 8. Thermodynamic consistency tests for LiC_6, given by Eq. (28) [x_α d ln γ_α/dx_α] with respect to x_α and [x_β d ln γ_β/dx_β] with respect to x_β.

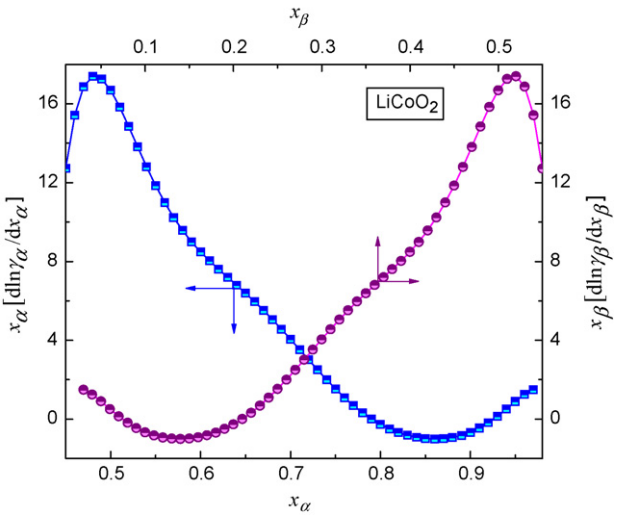

Fig. 9. Thermodynamic consistency tests for $LiCoO_2$, given by Eq. (28) [x_α d ln γ_α/dx_α] with respect to x_α and [x_β d ln γ_β/dx_β] with respect to x_β.

other as they are plotted with respect to their respective compositions ($x_\alpha + x_\beta = 1$). The value of x_α goes from 0.01 to 0.8. Thus x_β ranges from 0.99 to 0.2. Fig. 9 shows the thermodynamic consistency according to the Gibbs-Duhem equation for $LiCoO_2$ electrode, where x_α varies from 0.45 to 0.98. The numerical differences in the thermodynamic consistencies for both the electrodes were shown in Fig. 10.

6. Single Particle Li-ion Model

In a single particle model, the active electrode material of anode and cathode are assumed to be made up of uniform spherical particle. In this model, the area of the spherical particle is scaled to the active area of the solid phase in the porous electrode. The polarization losses in the solution phase are neglected. The Li transport inside the particle is only by diffusion mechanism. Further details of this model are explained in Refs. [28–31].

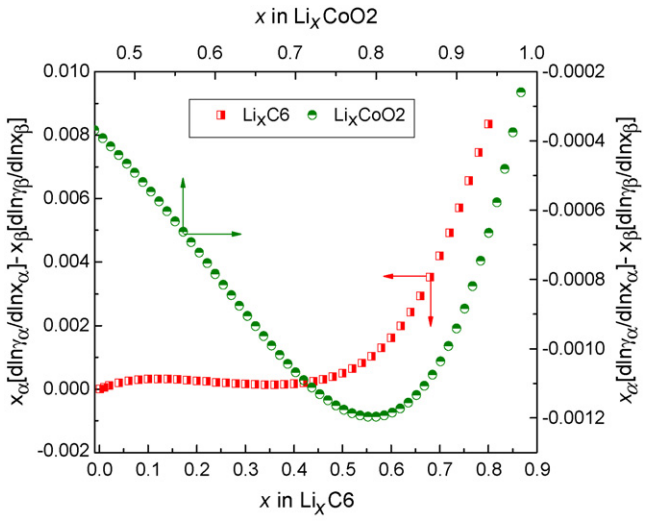

Fig. 10. The difference between the LHS and the RHS of the Gibbs-Duhem Eq. (28) for LiC_6 and $LiCoO_2$ electrode.

Reactions occurring at the surface of the two electrodes are:

$$\begin{aligned} &LiC_6 \underset{\text{charge}}{\overset{\text{discharge}}{\rightleftharpoons}} Li^+ + e^- + C_6 \\ &Li^+ + e^- + CoO_2 \underset{\text{charge}}{\overset{\text{discharge}}{\rightleftharpoons}} LiCoO_2 \end{aligned} \tag{29}$$

The driving force for flux is defined in the present work using the gradient of chemical potential [2,16] neglecting the effect of migration and convection

$$N_{\alpha,i} = -\frac{D_{\alpha,i}}{RT} c_{\alpha,i} \nabla \mu_{\alpha,i} \tag{30}$$

where α represents the lithium intercalated host material, β represents the unoccupied host material. Subscript i corresponds to positive or negative electrode (i = p or n, respectively). The effect of migration is neglected because the active material is generally a good electronic conductor.

Substituting the relationship between the chemical potential and the activity coefficient shown in Eq. (3) into Eq. (30), the flux expression can be derived as shown in Ref. [2] as

$$N_{\alpha,i} = -D_{\alpha,i} \left(1 + \frac{\mathrm{d} \ln \gamma_{\alpha,i}}{\mathrm{d} \ln x_{\alpha,i}}\right) \nabla c_{\alpha,i} \tag{31}$$

$(1 + ((\mathrm{d} \ln \gamma_{\alpha,i})/(\mathrm{d} \ln x_{\alpha,i})))$ represents the activity correction term; it is a strong function of the concentration of Li-ions, and often neglected [2]. The interactions with in the solid phase if neglected could not give a realistic representation of the intercalation process [16].

The activity correction term can be derived from Eq. (21) as

$$\left(1 + \frac{\mathrm{d} \ln \gamma_{\alpha,i}}{\mathrm{d} \ln x_{\alpha,i}}\right) = 1 + \sum_{k=0}^{N} 2A_k x_\alpha (1 - x_\alpha)(2x_\alpha - 1)^k \times \left[\frac{k(2x_\alpha k + x_\alpha - 1)}{(2x_\alpha - 1)^2} + (k+1)\right] \tag{32}$$

The general differential material balance in the absence of the reaction term is given by:

$$\frac{\partial c_{\alpha,i}}{\partial t} = -\nabla \cdot N_{\alpha,i} \tag{33}$$

Substituting the flux in the material balance for the spherical particle

$$\frac{\partial x_{\alpha,i}}{\partial t} = -\frac{D_{\alpha,i}}{R_i^2 \bar{R}^2} \frac{\partial}{\partial \bar{R}} \left[\bar{R}^2 \left(1 + \frac{\mathrm{d} \ln \gamma_{\alpha,i}}{\mathrm{d} \ln x_{\alpha,i}}\right) \frac{\partial x_{\alpha,i}}{\partial \bar{R}}\right] \tag{34}$$

where concentration ($c_{\alpha,i}$) is written in terms dimensionless mole fraction ($x_{\alpha,i}$) and dimensionless radius is given by $\bar{R} = r/R_i$.

The initial and the boundary conditions are:

$$\begin{aligned} &t = 0; && x_{\alpha,i} = x^0_{\alpha,i} \\ &\bar{R} = 0;\ t > 0; && \frac{\partial x_{\alpha,i}}{\partial \bar{R}} = 0 \\ &\bar{R} = 1;\ t > 0; && -D_{\alpha,i} c_{i,\max} \left(1 + \frac{\mathrm{d} \ln \gamma_{\alpha,i}}{\mathrm{d} \ln x_{\alpha,i}}\right) \frac{\partial x_{\alpha,i}}{\partial \bar{R}} = \pm \frac{I_{\text{app}} \bar{R}_i}{s_i F} \end{aligned} \tag{35}$$

The flux takes a positive value for i = p, negative for i = n.

Butler-Volmer equation is used to determine the kinetics of the intercalation process.

$$\pm \frac{I_{\text{app}}}{s_i F} = k_i [c_{\alpha,i,\max} - c_{\alpha,i}]^{1-\beta} [c_{\alpha,i} c_e]^\beta \times \left[\exp\left(\frac{(1-\beta)F}{RT} \eta_{s,i}\right) - \exp\left(\frac{-\beta F}{RT} \eta_{s,i}\right)\right] \tag{36}$$

The over potential ($\eta_{s,i}$) is defined as

$$\eta_{s,i} = \phi_i - \phi_e - U \tag{37}$$

Substituting the expression for U from Eq. (24) and applying Redlich-Kister equation we obtain

$$\eta_{s,i} = \phi_i - \phi_e - \left[U^0 + \frac{RT}{nF} \ln\left(\frac{1 - x_{\alpha,i}}{x_{\alpha,i}}\right) + V_{\text{INT}}\right] \tag{38}$$

$$\eta_{s,i} = \phi_i - \phi_e - \left[U^0 + \frac{RT}{nF} \ln\left(\frac{1 - x_{\alpha,i}}{x_{\alpha,i}}\right) + \frac{1}{nF} \left\{\sum_{k=0}^{N} A_k \cdot \left[(2x_{\alpha,i} - 1)^{k+1} - \frac{2x_{\alpha,i} k (1 - x_{\alpha,i})}{(2x_{\alpha,i} - 1)^{1-k}}\right]\right\}\right] \tag{39}$$

ϕ_i is the solid phase potential. The solution phase potential (ϕ_e) is equated to zero based on the assumptions of the single particle model. The term c_e refers to the concentration of the electrolyte. β is the symmetry factor which represents the fraction of applied potential that promote the cathodic reaction, and $(1 - \beta)$ is the fraction of potential applied that promotes the anodic reaction. In general the symmetry factor (β) takes the value of 0.5.

The equilibrium potential expression which includes the interaction term corrects the Butler-Volmer (BV) equation for the non-ideal behavior. Dimensionless form of the BV equation is given as

$$\pm \frac{I_{\text{app}}}{s_i F c_e^{0.5} k_i c_{\alpha,i,\max}} = [1 - x_{\alpha,i}]^{1-\beta} [x_{\alpha,i}]^\beta \left[\exp\left(\frac{(1-\beta)F}{RT} \eta_{s,i}\right) - \exp\left(\frac{-\beta F}{RT} \eta_{s,i}\right)\right] \tag{40}$$

The theoretical electroactive area of the single spherical particle scaled to the porous electrode is given by

$$s_i = \frac{3 w_i}{R_i \rho_i} \tag{41}$$

where w_i and ρ_i are the weight and the density of the active material inside electrode (i), respectively.

The activity correction term given in Eq. (32) was plotted for $LiCoO_2$ and MCMB as a function of stoichiometric coefficient in Fig. 11. In the case of $LiCoO_2$, the activity correction term increases to a higher value at initial stoichiometry. This is because the intercalated Li-ions occupy a vacant space available in the host matrix randomly. Then the activity correction term decreases during the transition between the disordered to an ordered lattice structure. An ordered lithium super lattice occurs around 4.15 V corresponding to the x value of 0.53 [25]. The correction term decreases to a lower value in the entire two phase region (x = 0.75 to 0.95). Finally it increases when the lithium rich single phase was formed at the end of discharge. The diffusion of lithium into the host was limited due to the higher concentration of lithium ions in the CoO_2 matrix. For the MCMB, in the region of dilute stage 1 [5] the activity correction term has a higher value and then starts to decrease rapidly during the transition from dilute stage 1 to stage 4, due to the ordering effects. The correction term increase during the transitions from stage 4 to liquid type stage 2 at x = 0.18, and decreases during the transition from liquid type stage 2 to stage 2 at x = 0.3 due to ordering effects. The correction term decreases to a lower value in the two phase region during stage 2 to stage 1 transition.

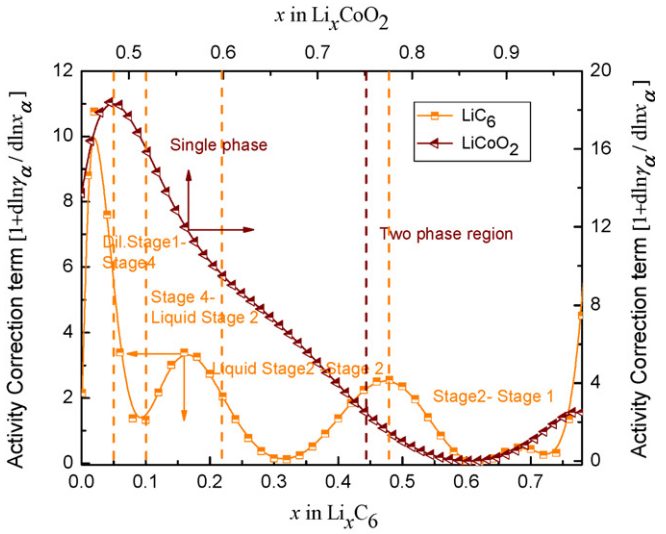

Fig. 11. Activity correction term $(1 + \mathrm{d}\ln\gamma_\alpha/\mathrm{d}\ln x_\alpha)$ for LiC_6 and $LiCoO_2$ electrode with respect to composition obtained by substituting the parameters in Eq. (32).

The effective diffusivity was defined as the product of the diffusion coefficient with the activity correction term [2].

$$D_{\mathrm{eff},i} = D_{\alpha,i}\left(1 + \frac{\mathrm{d}\ln\gamma_{\alpha,i}}{\mathrm{d}\ln x_{\alpha,i}}\right) \tag{42}$$

The effective diffusivity depends upon the ordered to disordered transitions occurring during the lithium intercalation and deintercalation process [16]. The effect of change in the solid phase effective diffusivity for $LiCoO_2$ and MCMB on the charge and discharge process is analyzed using the single particle model. The governing Eq. (34) along with the boundary conditions and the Butler-Volmer expression (Eqs. (35) and (36), respectively) were solved for both the electrodes simultaneously using COMSOL Multiphysics®. The parameters are taken from MSA Li-ion cell and are presented in Table 8. Figs. 12 and 13 compares the discharge and charge profiles, respectively as the function of cell capacity using the single particle model, with and without the activity correction term. The effect of activity correction is not pronounced at low rates of discharge. However at higher discharge rates, there is a notable difference in the capacity and charge/discharge profiles. This is because at higher rates the solid phase diffusion limitation plays a significant role in discharge process. Neglecting the activity correction term underestimates the effective diffusivity and therefore a lesser predicted capacity is observed. At 1C rate, the capacity differs by as much as 10%. Table 9 compares the difference in the discharge capacity between activity corrected model and the activity ignored model.

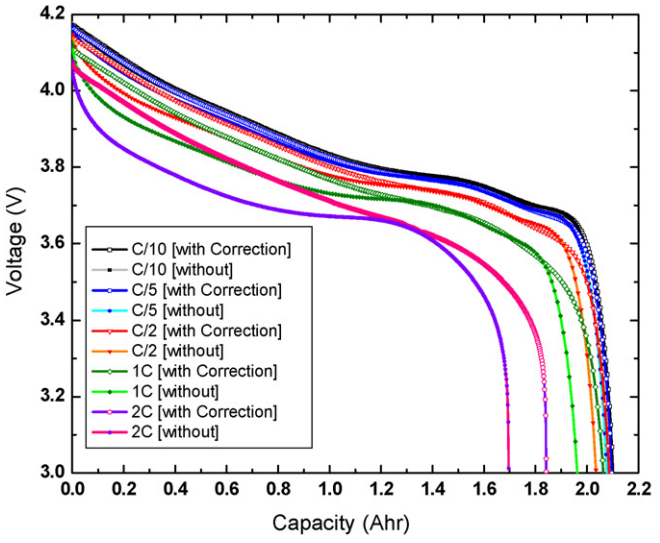

Fig. 12. Comparison of cell voltage vs. discharge capacity with and without activity correction term at C/10, C/5, C/2, 1C and 2C rates. The open symbols represent the activity corrected model, and the solid symbols represent the diffusion model without correction factor (1.656 A cm^{-2} for 1C rate).

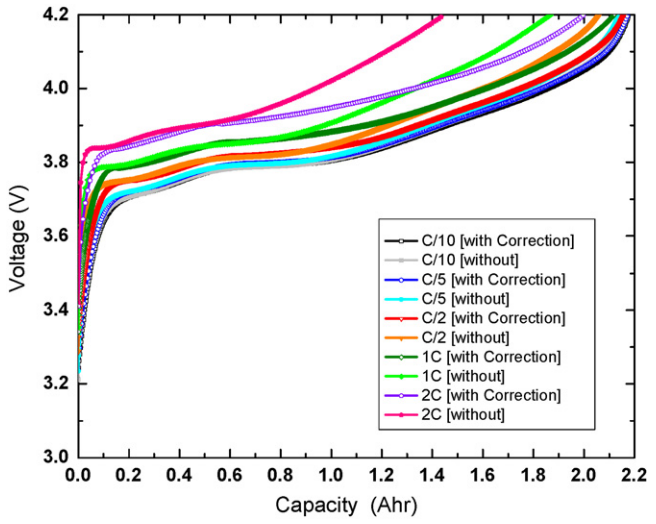

Fig. 13. Comparison of cell voltage vs. charge capacity with and without activity correction term at C/10, C/5, C/2, 1C and 2C rates. The open symbols represent the activity corrected model, and the solid symbols represent the diffusion model without correction factor. (1.656 A cm^{-2} for 1C rate).

Figs. 14 and 15 shows the concentration profile of Li-ion with time across the dimensionless radius of the MCMB and $LiCoO_2$ respectively at 1C discharge rate for the full cell, with and without the correction factor. The dimensionless concentration of Li-ions begins at 0.8 when $t = 0$ and decreases with increase in time (Fig. 14) as Li-ion de-intercalates from the MCMB particle during discharge. When the activity correction is included in the model, ridges are observed in the concentration profile in the regions where the dimensionless concentration equals 0.3 and 0.6. This is because the solid phase diffusion coefficient of Li-ion varies according to the Eq. (42) and is proportional to the activity correction term. For MCMB, the activity correction term decreases in the two phase region ($x = 0.3$ and 0.6) and so is the effective diffusivity. Thus the steep segments in the concentration profile are attributed to the stage transition with in the MCMB. In case of $LiCoO_2$, the dimensionless Li-ions concentration increases as Li-ions intercalates during discharge. Similar to MCMB high gradients are observed in the concentration profile due to the formation of two phase region at $x = 0.85$, where the effective diffusivity is low.

Table 9
The difference in the discharge capacity predicted by the single particle model with and without the activity correction term

Rates	Approximate difference
C/10	<1%
C/5	2%
C/2	5%
1C	10%
2C	15%

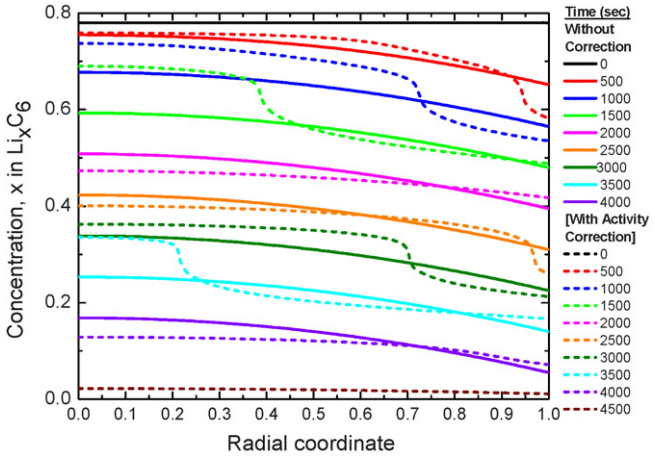

Fig. 14. Concentration profile across the MCMB particle at 1C discharge rate, with and without the correction term.

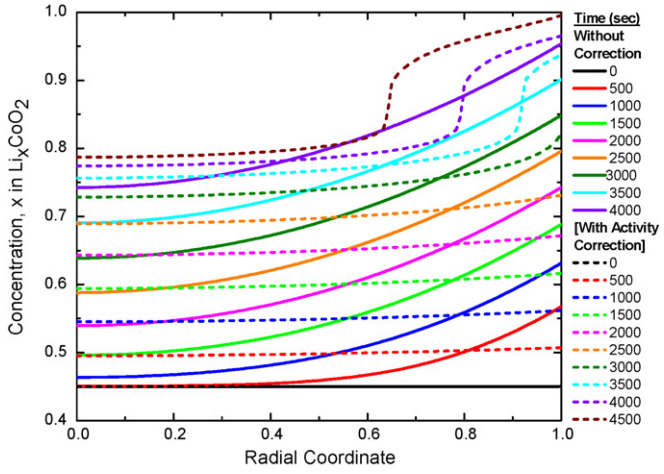

Fig. 15. Concentration profile across the $LiCoO_2$ particle at 1C discharge rate, with and without the correction term.

7. Conclusions

A thermodynamic relation using Redlich-Kister equation was developed to describe the concentration dependence of equilibrium potential of lithium intercalation electrodes. The excess Gibbs free energy defined by Redlich-Kister equation was also used to evaluate the activity correction term. The corrected activity term was used to define the non-ideal chemical potential of the intercalation species to define the flux. These non-idealities were incorporated into a single particle model and was used to simulate the charge and the discharge behavior of MCMB–$LiCoO_2$ system. The effect of different charge and discharge rates on the voltage profile and capacity were analyzed. The inclusion of activity coefficient correction in the single particle model predicted a higher capacity and the effect was more pronounced at higher rates. The inclusion of the activity correction term was realized through an effective diffusivity term, which largely determines the concentration profile and the capacity.

References

[1] K. West, T. Jacobsen, S. Atlung, J. Electrochem. Soc. 129 (1982) 1480–1485.
[2] M.W. Verbrugge, B.J. Koch, J. Electrochem. Soc. 143 (1996) 600–608.
[3] M.W. Verbrugge, B.J. Koch, J. Electrochem. Soc. 150 (2003) A374–A384.
[4] T. Ohzuku, A. Ueda, J. Electrochem. Soc. 144 (1997) 2780–2785.
[5] R. Yazami, Y. Reynier, J. Power Sources 153 (2006) 312–318.
[6] Q.Z. Guo, R.E. White, J. Electrochem. Soc. 152 (2005) A343–A350.
[7] N. Yabuuchi, Y. Makimura, T. Ohzuku, J. Electrochem. Soc. 154 (2007) A314–A321.
[8] S.A.H. Ali, Ionics 11 (2005) 410–413.
[9] M. Doyle, J. Newman, A.S. Gozdz, C.N. Schmutz, J.M. Tarascon, J. Electrochem. Soc. 143 (1996) 1890–1903.
[10] G. Sikha, B.N. Popov, R.E. White, J. Electrochem. Soc. 151 (2004) A1104–A1114.
[11] P. Ramadass, B. Haran, R. White, B.N. Popov, J. Power Sources 123 (2003) 230–240.
[12] Q. Zhang, Q.Z. Guo, R.E. White, J. Electrochem. Soc. 153 (2006) A301–A309.
[13] R. Barnard, C.F. Randell, F.L. Tye, J. Appl. Electrochem. 10 (1980) 127–141.
[14] D.Y. Fan, R.E. White, J. Electrochem. Soc. 138 (1991) 2952–2960.
[15] M. Jain, A.L. Elmore, M.A. Matthews, J.W. Weidner, Electrochim. Acta 43 (1998) 2649–2660.
[16] G.G. Botte, R.E. White, J. Electrochem. Soc. 148 (2001) A54–A66.
[17] J. Christensen, J. Newman, J. Solid State Electrochem. 10 (2006) 293–319.
[18] R. Kanno, Y. Kawamoto, Y. Takeda, S. Ohashi, N. Imanishi, O. Yamamoto, J. Electrochem. Soc. 139 (1992) 3397–3404.
[19] J.M. Prausnitz, Molecular Thermodynamnics of Fluid Phase Equilibria, Prentice Hall, NJ, 1986.
[20] G. Prentice, Electrochemical Engineering Principles, Prentice-Hall, NJ, 1991.
[21] S.M. Walas, Phase Equilibria in Chemical Engineering, Butterworth, MA, 1985.
[22] A. Constantindis, N. Mostoufi, Numerical Methods for Chemical Engineers with MATLAB Applications, Prentice-Hall, NJ, 1999.
[23] T. Ohzuku, Y. Iwakoshi, K. Sawai, J. Electrochem. Soc. 140 (1993) 2490–2498.
[24] Y.F. Reynier, R. Yazami, B. Fultz, J. Electrochem. Soc. 151 (2004) A422–A426.
[25] J.N. Reimers, J.R. Dahn, J. Electrochem. Soc. 139 (1992) 2091–2097.
[26] Z.H. Chen, Z.H. Lu, J.R. Dahn, J. Electrochem. Soc. 149 (2002) A1604–A1609.
[27] Q. Zhang, R.E. White, J. Electrochem. Soc. 154 (2007) A587–A596.
[28] B.S. Haran, B.N. Popov, R.E. White, J. Power Sources 75 (1998) 56–63.
[29] G. Ning, B.N. Popov, J. Electrochem. Soc. 151 (2004) A1584–A1591.
[30] S. Santhanagopalan, Q.Z. Guo, P. Ramadass, R.E. White, J. Power Sources 156 (2006) 620–628.
[31] S. Santhanagopalan, Q.Z. Guo, R.E. White, J. Electrochem. Soc. 154 (2007) A198–A206.